

Article

# Bifocal Dual-Reflectarray Antenna to Generate a Complete Multiple Spot Beam Coverage for Satellite Communications in Ka-Band

Eduardo Martinez-de-Rioja <sup>1,\*</sup>, Jose A. Encinar <sup>2</sup> and Giovanni Toso <sup>3</sup>

<sup>1</sup> Area of Signal Theory and Communications, Universidad Rey Juan Carlos, 28943 Fuenlabrada, Spain

<sup>2</sup> Information Processing and Telecommunications Center, Universidad Politécnica de Madrid, 28040 Madrid, Spain; jose.encinar@upm.es

<sup>3</sup> Antenna and Sub-Millimeter Wave Section, European Space Agency ESTEC, 2200 AG Noordwijk, The Netherlands; giovanni.toso@esa.int

\* Correspondence: eduardo.martinez@urjc.es

Received: 13 May 2020; Accepted: 6 June 2020; Published: 9 June 2020



**Abstract:** This paper presents a novel multibeam transmitting dual-reflectarray antenna able to generate a complete multiple spot coverage from a geostationary satellite in Ka-band (20 GHz). The bifocal design technique has been exploited for the first time to reduce by 50% the beam deviation factor with respect to the equivalent monofocal antenna, allowing to produce adjacent beams separated by only  $0.56^\circ$  in the antenna offset plane. In order to guarantee an acceptable spillover, the main reflectarray has been oversized in the same plane where the beams are compressed, resulting in an elliptical reflectarray of  $3.5\text{ m} \times 1.8\text{ m}$ . The interleaved beams required to provide the complete multi-spot coverage are produced in the orthogonal polarization, using the same aperture and feeds. The proposed antenna requires a smaller main aperture (about half of the area) and a lower number of feeds than other configurations that use a single oversized reflector to generate a complete multi-spot coverage, showing promising results for communication satellite applications in the Ka-band.

**Keywords:** bifocal antennas; dual-reflectarray antennas; Ka-band; multibeam antennas; multispot coverage; satellite communications

## 1. Introduction

The development of high throughput satellites (HTS) in the Ka-band has originated an increased interest in novel multiple beam antenna architectures [1–3]. Current HTS systems provide a cellular coverage formed by a large number of closely-spaced spot beams, according to a multi-color reuse scheme [1]. Reflector antennas in single feed per beam (SFPB) configuration provide high gain and bandwidth, but they cannot produce all the beams satisfying the required conditions in terms of spillover, limited side-lobe level and sufficient isolation. The inter-feed spacing imposed by the small beam separation (a typical value is  $0.56^\circ$ ) is not compatible with the feed diameter required for the efficient illumination of the reflector [2]. To circumvent this limitation, four reflectors operating in transmission (Tx) and reception (Rx) in a SFPB scheme are usually adopted, so that the adjacent beams are produced by different reflectors [2,3]. One of the main drawbacks of this multibeam antenna configuration is associated to the volume required to accommodate four large reflectors (between 2 m and 2.5 m in diameter) on the satellite.

Different solutions have been investigated to produce a complete multibeam coverage using a single main aperture [4]. The use of a single reflector to produce all the beams in a SFPB scheme results in a highly oversized reflector, around 4 m in diameter, with a large focal distance [5]. The area of the oversized reflector is comparable to the total area of the standard four-reflector system, so it exhibits

similar accommodation problems. Moreover, the oversized reflector has to be significantly shaped in order to produce a larger beamwidth, which implies higher manufacturing costs [5]. Another type of multibeam antenna is represented by the so-called multiple feed per beam (MFPB) architecture, where the beams are generated by subarrays overlapped in the focal region. MFPB systems permit reducing the number of antennas on board the satellite [6,7], but they present some drawbacks associated to the complex and expensive beamforming networks that feed the antennas. In practice, this class of antenna has been used, up to now, to generate a limited number of beams with slightly inferior electrical performance as compared to SFPB systems [3,6]. Multibeam antennas based on direct radiating arrays [8,9] and active lenses [10] have also been investigated, but they are typically highly complex and costly. Another promising antenna architecture, which exhibits less mechanical complexity, is based on the use of quasi-optical beamformers that feed a multibeam lens or reflector system [11–13].

Reflectarray antennas combine their capability to generate independent beams in different polarizations [14,15] or frequencies [16,17] with the hardware simplicity of SFPB systems. In fact, the generation of two beams per feed (associated to two polarizations [18] or two frequencies [19]) can lead to a reduction in the number of apertures required to provide a complete multibeam coverage. Recently, a novel bifocal design technique has been developed for dual-reflectarray antennas (DRAAs) in offset configurations [20], which allows improving the multibeam performance of the antenna for Ka-band satellite applications.

In this paper, the authors present the design of a bifocal DRAA to generate a complete multiple spot beam coverage with a single main aperture, for transmission from a geostationary (GEO) satellite operating in the Ka-band. The bifocal technique has been applied for the first time to obtain a significant reduction of the beam deviation factor in the offset plane (i.e., a reduction by 50%) with respect to the equivalent monofocal antenna. The main reflectarray has been oversized in the same dimension where the beams are going to be compressed in order to reduce the spillover, resulting in an elliptical reflectarray of dimensions 3.5 m × 1.8 m. The interleaved beams required to provide the full coverage will be generated in the orthogonal polarization by exploiting the dual-polarization capability of the reflectarray elements. The proposed bifocal DRAA represents an improved solution with respect to the 4 m oversized SFPB reflector [5], since it requires a smaller aperture size, employs a lower number of feeds, and shows larger radiation efficiency. The replacement of the standard multi-reflector architecture by the proposed bifocal DRAA could enable a significant reduction in cost, volume and weight of the antenna farm for HTS systems operating in the Ka-band.

## 2. Multibeam Bifocal Dual-Reflectarray Antennas in Ka-Band

For many years, the bifocal technique has been applied to the design of dual-reflector systems to obtain an improved multibeam and beam scanning performance [21–24]. Bifocal antennas provide better results for the extreme beams in terms of gain and side-lobe levels, resulting in reduced scan loss and lower interference levels than their monofocal counterparts [21,25]. Moreover, the bifocal algorithm allows a certain degree of control in the angular separation between adjacent beams (through the election of the beam directions associated to the focal points), which has traditionally been used to increase the beam deviation factor with respect to the equivalent monofocal antenna for wide-angle beam scanning applications [22–25].

Recently, the bifocal concept has been applied to DRAA systems formed by flat reflectarrays [20,26]. A general 3D bifocal method has been presented in [20] for the design of offset DRAA configurations, with application to multibeam satellite antennas. The bifocal method has been validated by the fabrication and testing of the first offset bifocal DRAA prototype [20], which consists of a 57 cm × 42 cm main reflectarray (main RA) and a 39 cm × 35 cm sub-reflectarray (sub-RA) in an offset compact-range configuration, see Figure 1a. The DRAA demonstrator has been designed with reflectarray cells that enable independent phase control in each polarization, so the antenna is able to generate two adjacent beams in orthogonal polarization per feed at the Tx frequencies in the Ka-band (19.2–20.2 GHz). Figure 1b shows the simulated and measured radiation patterns in the offset plane for the 10 beams

produced by 5 adjacent feeds (note that the beams alternate in polarization). A scaled version of this prototype with a 1.8 m main RA can be designed to produce multiple beams in the Ka-band from a GEO satellite [20], resulting in the feed and beam configurations shown in Figure 1c,d, respectively. The final separation between adjacent beams (in orthogonal polarization) in the same plane “ $v = \text{constant}$ ” would be  $0.56^\circ$ . However, the feed diameter imposes some restrictions in the beam spacing achieved in the orthogonal plane, so the antenna would be able to produce only one half of the multibeam coverage, and a second multibeam DRAA (designed with the same technique) should be used to produce the other half of the coverage.

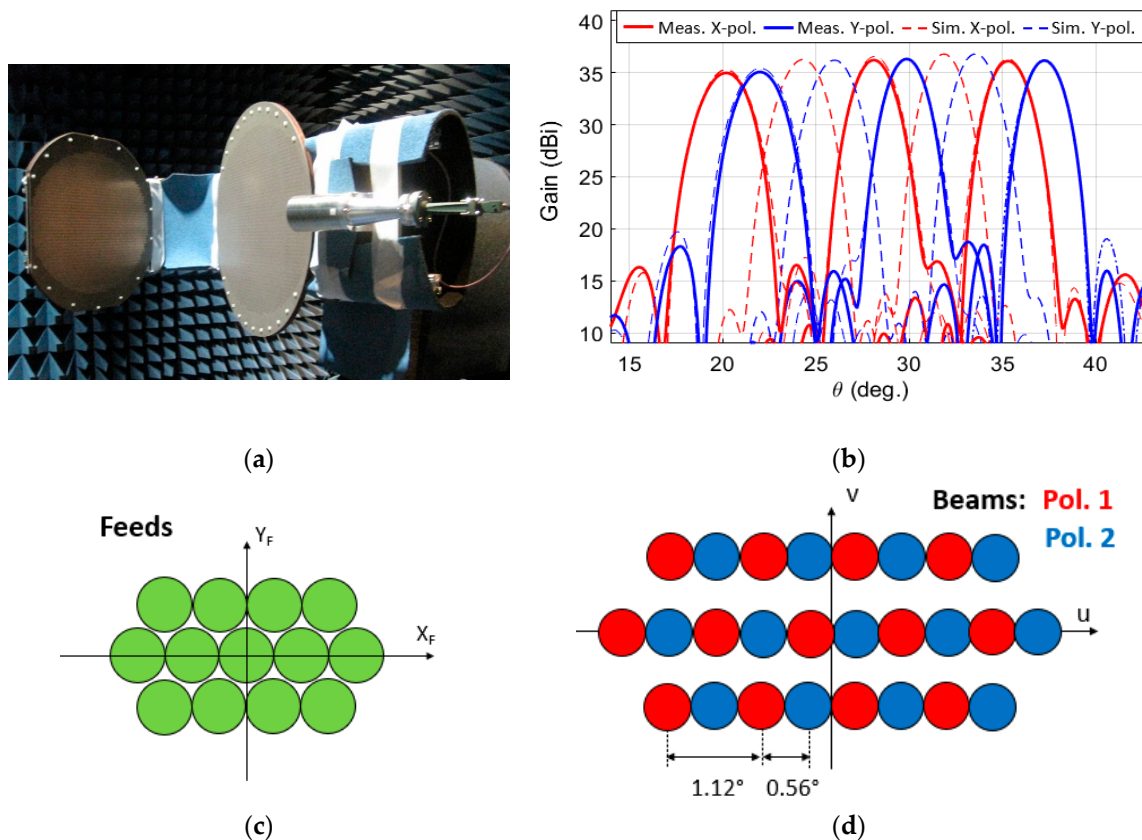


**Figure 1.** (a) Manufactured bifocal dual-reflectarray antenna (DRAA) demonstrator, (b) simulated and measured radiation patterns at 19.7 GHz of the 10 beams produced by 5 adjacent horns operating in dual polarization, (c) feed cluster and (d) beam configuration associated to the bifocal DRAA proposed in [20].

This paper presents a novel multibeam transmitting DRAA designed to generate a complete multiple spot beam coverage with a single main aperture, see Figure 2. In contrast to the previous bifocal antennas [21–26], which are designed to provide a larger beam spacing (or similar beam spacing) than the equivalent monofocal antenna, the bifocal technique has been applied for the first time here to achieve a significant reduction of the beam deviation factor (around 50% reduction). This allows achieving  $0.56^\circ$  angular spacing in the offset plane between the beams produced in the same polarization by adjacent feeds. The bifocal antenna does not provide any beam spacing reduction in the orthogonal plane, so the interleaved beams required to complete the coverage will be generated in the orthogonal polarization by exploiting the dual-polarization capability of the reflectarray elements. Hence, each feed will produce two adjacent beams in orthogonal polarization, in a plane forming around  $60^\circ$  with the “ $v = 0$ ” plane, see Figure 2b,c. In order to avoid the high interference of a two-color coverage scheme, the 1 GHz band allocated for Tx (19.5–20.5 GHz) can be divided into two sub-bands of 500 MHz, with central frequencies of 19.75 GHz and 20.25 GHz, so that the adjacent feeds will

alternate in frequency. Thus, the adjacent beams in the same plane “ $v = \text{constant}$ ” (generated in the same polarization by different feeds) will alternate in frequency.

In previous applications of the bifocal technique with similar beam spacing to that of the monofocal case, no significant impact in the antenna gain and efficiency was observed, which allowed keeping the same aperture size as in the equivalent monofocal antenna [20–22,25]. However, the application of the bifocal method for a high degree of beam spacing reduction, as proposed in this paper, leads to a larger spillover on the main RA and to a reduced radiation efficiency. To overcome this problem, the main RA has been oversized in the same dimension where the beam spacing is going to be reduced, resulting in an elliptical main RA of dimensions  $3.55 \text{ m} \times 1.81 \text{ m}$ .

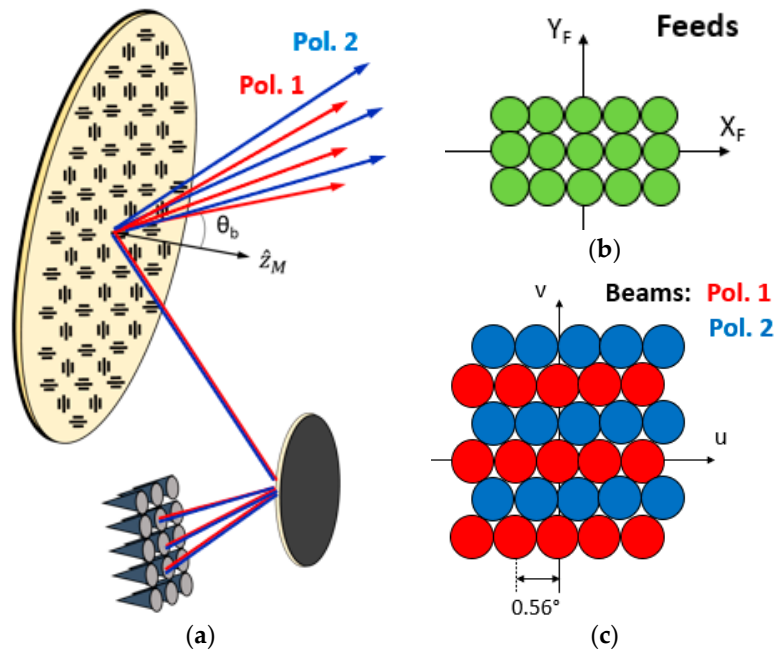


**Figure 2.** (a) Proposed bifocal DRAA configuration with an elliptical main reflectarray (RA) to produce multiple adjacent beams in dual polarization, (b) feed cluster and (c) beam configuration associated to the proposed antenna to produce a complete multibeam coverage in the Ka-band.

### 3. Design of the Bifocal DRAA Configuration

The proposed DRAA system has been designed by adopting a Cassegrain configuration, as can be seen in Figure 3. The main geometrical parameters of the DRAA are given in Table 1. The antenna consists of an elliptical flat main-RA of size  $3.55 \text{ m} \times 1.81 \text{ m}$ , and a circular flat sub-RA of 79 cm diameter, with a relative tilting of  $10^\circ$  between them. An array of five adjacent feed-horns placed in the  $xz$ -plane (the antenna symmetry plane) was initially considered for the antenna illumination (feeds  $F_1$  to  $F_5$  in Figure 3), which corresponds to the central row of feeds in Figure 2b. A realistic model of a Ka-band feed-horn [3] has been used: the horns have a diameter of 54 mm and provide around  $-12 \text{ dB}$  illumination on the sub-RA edges at 20 GHz for a subtended angle of  $36^\circ$ .

The proposed DRAA geometry has been derived from a Cassegrain dual-reflector configuration, where both reflectors have been replaced by flat reflectarrays. The equivalent parabolic reflector for the elliptical flat main-RA presents the following parameters: dimensions (projected)  $3.36 \text{ m} \times 1.81 \text{ m}$ , focal distance  $F = 4.72 \text{ m}$ , and clearance  $C = 1.57 \text{ m}$ . The focal location for the equivalent parabolic reflector coincides with the position of the virtual focus related to the central feed ( $F_3$ ) of the proposed antenna. The phase center of  $F_3$  has been placed at the real focus of the Cassegrain system, and then, the adjacent feeds ( $F_1$ ,  $F_2$ ,  $F_4$  and  $F_5$ ) have been situated with a separation of 55 mm between their phase centers (allowing 1 mm margin to properly accommodate the horns). The sub-RA dimensions and tilting angle have been finely adjusted after carrying out a trade-off with the bifocal algorithm,

in order to ensure an appropriate illumination on the main RA when the bifocal technique is applied to reduce the beam deviation factor and obtain closer beams (separated by  $0.56^\circ$ ), at the same time as avoiding the blockage from the sub-RA and the feed-horns. Note that the Cassegrain system allows working with a smaller sub-RA size than in the case of the compact-range system used in [20,27]. A cell period of 10 mm has been considered for both reflectarrays to avoid working with an excessive number of reflectarray elements; however, in a realistic design the period should be lower (e.g., around  $\lambda/2$  at 20 GHz) to avoid grating lobes and to provide larger bandwidth.

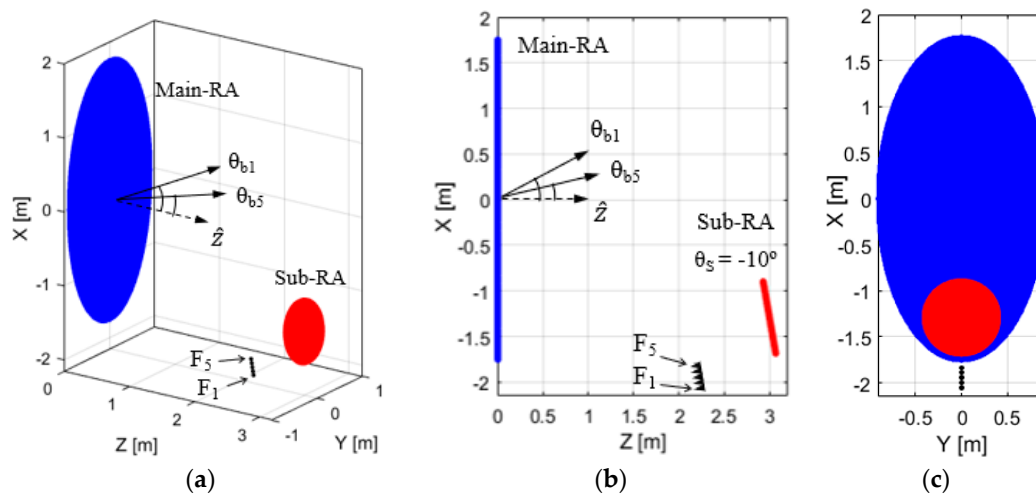


**Figure 3.** Geometry of the proposed DRAA configuration, formed by an elliptical main RA and a circular sub-reflectorarray: (a) 3D view, (b) lateral view and (c) front view.

**Table 1.** Geometric parameters of the DRAA configuration.

Parameter	Value
Size Main-RA	3.55 m $\times$ 1.81 m
Size Sub-RA	0.79 m $\times$ 0.79 m
Angle of tilting Sub-RA	$10^\circ$
Geometrical center Main-RA	[0, 0, 0] mm
Geometrical center Sub-RA	[-1288, 0, 3003] mm
Phase center of feed $F_1$	[-2043, 0, 2222] mm
Phase center of feed $F_3$	[-1937, 0, 2204] mm
Phase center of feed $F_5$	[-1830, 0, 2185] mm
Virtual focus related to $F_3$	[-1854, 0, 4847] mm

A reference monofocal design of the proposed DRAA system has been carried out at 20 GHz, considering that the antenna focus is placed at the phase center of the central feed ( $F_3$ ), whose associated beam will radiate in the direction  $\theta_{b3} = 19^\circ$ ,  $\varphi_{b3} = 0^\circ$  with respect to the normal vector to the main-RA surface. The monofocal phase distribution required on the sub-RA has been computed from the phase delay associated to the difference between two paths: the path between the phase center of  $F_3$  and the sub-RA plane, and the path between the virtual focus related to  $F_3$  and the sub-RA plane. Then, the monofocal phase distribution on the main RA has been obtained from the progressive phase distribution that generates the required focused beam, considering that the feed was placed at the virtual focus. The resultant monofocal phase distributions for both reflectarrays are depicted in Figure 4. The monofocal DRAA will provide around  $1.1^\circ$  of beam spacing (as will be shown later). Since the feed-horns are placed adjacent to each other, a smaller beam spacing would require overlapping feeds. Note also that a conventional monofocal DRAA would employ a circular main RA of 1.8 m diameter instead of an elliptical one. As stated before, the reason for oversizing the main RA is related to the application of the bifocal technique to reduce the beam spacing in the  $xz$ -plane by a large factor.

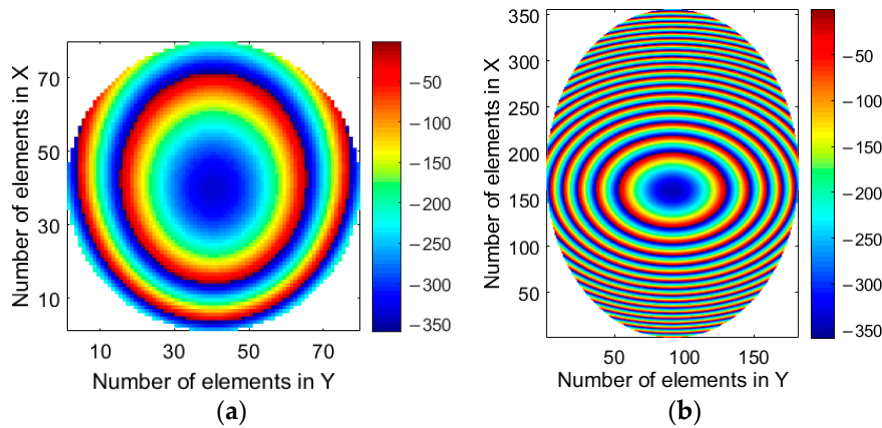


**Figure 4.** Monofocal phase distributions (in degrees) on (a) the sub-RA and (b) the main RA.

The bifocal technique has been applied to the proposed DRAA configuration in order to obtain  $0.56^\circ$  separation between adjacent beams in the  $xz$ -plane, which involves a large reduction of the beam deviation factor (by a factor close to 2) with respect to the equivalent monofocal DRAA. The two focal points of the bifocal antenna have been selected to match the phase centers of the feeds  $F_1$  and  $F_5$  depicted in Figure 3. The beam directions associated to each focus have been chosen as  $\theta_{b1} = 20.12^\circ$ ,  $\varphi_{b1} = 0^\circ$  and  $\theta_{b5} = 17.88^\circ$ ,  $\varphi_{b5} = 0^\circ$ , in order to avoid blockage from the sub-RA and to provide  $0.56^\circ$  separation between beams produced by adjacent feed-horns.

The computation of the bifocal phase distributions required on both reflectarrays has been performed by means of an iterative ray-tracing algorithm, which alternates transmitted rays from  $F_1$  (the first focus of the DRAA) with received rays that are directed to  $F_5$  (the second focus). A detailed description of the ray-tracing algorithm can be found in [20]. The rays coming from  $F_1$  are reflected, first, by the sub-RA, and then, by the main RA, leaving the structure with an angle  $(\theta_{b1}, \varphi_{b1})$ . On the other hand, the received rays coming at an angle  $(\theta_{b5}, \varphi_{b5})$  are reflected, first, by the main RA, and then, by the sub-RA, being finally directed to  $F_5$ . When the rays impinge on the surface of the sub-RA or the main RA, the following equations are applied, which relate the angles of incidence  $(\theta_{inc}, \varphi_{inc})$  and reflection  $(\theta_{ref}, \varphi_{ref})$  of the rays with the partial derivatives of the bifocal phase distribution  $(\Phi_{bifocal})$  with respect to the longitudinal and transversal length variables:

$$\frac{\partial \Phi_{bifocal}(x, y)}{\partial x} = \frac{2\pi}{\lambda} \cdot (\sin \theta_{inc} \cos \varphi_{inc} - \sin \theta_{ref} \cos \varphi_{ref}) \tag{1}$$

$$\frac{\partial \Phi_{bifocal}(x, y)}{\partial y} = \frac{2\pi}{\lambda} \cdot (\sin \theta_{inc} \sin \varphi_{inc} - \sin \theta_{ref} \sin \varphi_{ref}) \tag{2}$$

The phases from the previous monofocal DRAA design have been used to obtain the initial conditions for the phase derivatives along the cross-section of both reflectarrays (parallel to the  $y$ -axis), as explained in [20]. This will allow keeping the monofocal characteristic of the DRAA in the azimuth plane, which will be combined with a bifocal design in the  $xz$ -plane to provide closer beams (separated by  $0.56^\circ$ ). After several iterations of the ray-tracing procedure, a set of phase derivative samples is obtained on the surface of both reflectarrays. The phase derivative samples are interpolated by polynomials, and then integrated to obtain the bifocal phase distributions that must be implemented on both reflectarrays. The resultant phase distributions obtained by this technique can be seen in Figure 5. Note that the main RA presents a larger number of  $360^\circ$  cycles along its vertical axis than in the monofocal design, while the sub-RA phases have changed from a convex to a concave characteristic (both effects are produced by the large degree of reduction in the beam spacing).

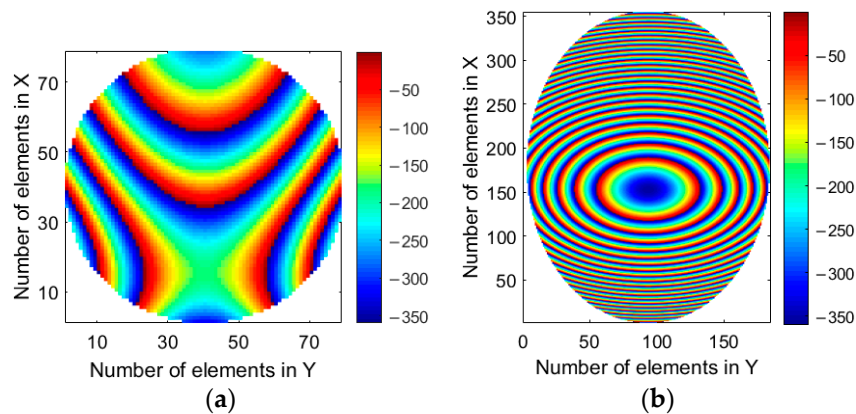


**Figure 5.** Bifocal phase distributions (in degrees) on (a) the sub-RA and (b) the main-RA.

The bifocal DRAA has been simulated using an in-house analysis software, assuming ideal reflectarray cells in both surfaces that provide the required phase-shift. The electromagnetic field radiated by the horns has been modeled using a  $\cos^q(\theta)$  function with  $q = 28$ , which provides  $-12$  dB illumination on the sub-reflectarray edges for a  $36^\circ$  subtended angle. The accuracy of the analysis and design software has been validated in previous works with satisfactory results [20,27], including the design, fabrication and testing of several DRAA prototypes in the Ku and Ka bands. The comparison of the radiation patterns in the  $xz$ -plane at 20 GHz with the beams generated by the bifocal DRAA (in solid colored lines) and those produced by the equivalent reference monofocal DRAA (in dashed lines) is shown in Figure 6.

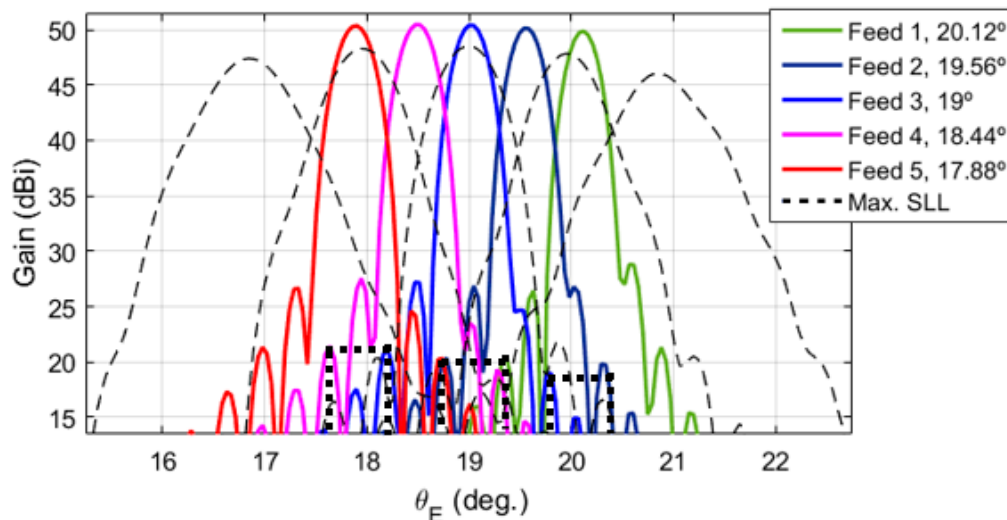


**Figure 6.** Simulated radiation patterns at 20 GHz in the  $xz$ -plane of the beams generated by the bifocal DRAA (solid colored lines) and the beams produced by the equivalent monofocal DRAA (dashed lines), indicating the maximum side-lobe levels (SLL, in black dotted lines) that produce the interference among reuse beams (see Section 5).

The separation between adjacent beams in the  $xz$ -plane is  $0.56^\circ$  for the bifocal DRAA, while it is around  $1^\circ$ – $1.1^\circ$  for the monofocal DRAA. The gain of the bifocal beams varies from 50.44 dBi to 49.85 dBi, the scan loss is 0.59 dB, and the side-lobe levels are lower than  $-21$  dB with respect to the maximum. On the other hand, the scan loss in the monofocal antenna is 2.5 dB (the gain varies from 48.5 dBi to 46 dBi) and the extreme beams are quite broadened. Note that the gain of the bifocal beams is a couple of dB higher than the gain of the monofocal beams, since the use of an oversized main RA produces narrower beams. According to these results, the bifocal DRAA is able to produce much closer

beams in the  $xz$ -plane than the reference monofocal antenna (beam spacing is reduced by a factor close to 2) with lower scan loss.

The radiation patterns of the bifocal DRAA in the azimuth plane (orthogonal to the  $xz$ -plane) are determined by the performance of the equivalent monofocal antenna, whose phase distributions have been used as initial conditions for the bifocal synthesis. Hence, the beam spacing provided by the bifocal DRAA in the azimuth plane is similar to that of the monofocal DRAA. This can be checked in Figure 7, which shows the comparison of the radiation patterns at 20 GHz in the azimuth plane for the bifocal DRAA (in solid lines) and the monofocal DRAA (in dashed lines), considering two additional beams produced by two horns placed adjacent to  $F_3$  ( $F_{3L}$  and  $F_{3R}$ ). The separation between adjacent beams is around  $1.1^\circ$  for both antennas, which is almost twice the angular spacing achieved in the  $xz$ -plane by the bifocal antenna. Thus, the bifocal antenna preserves the monofocal characteristic of the reference DRAA design in the azimuth plane.

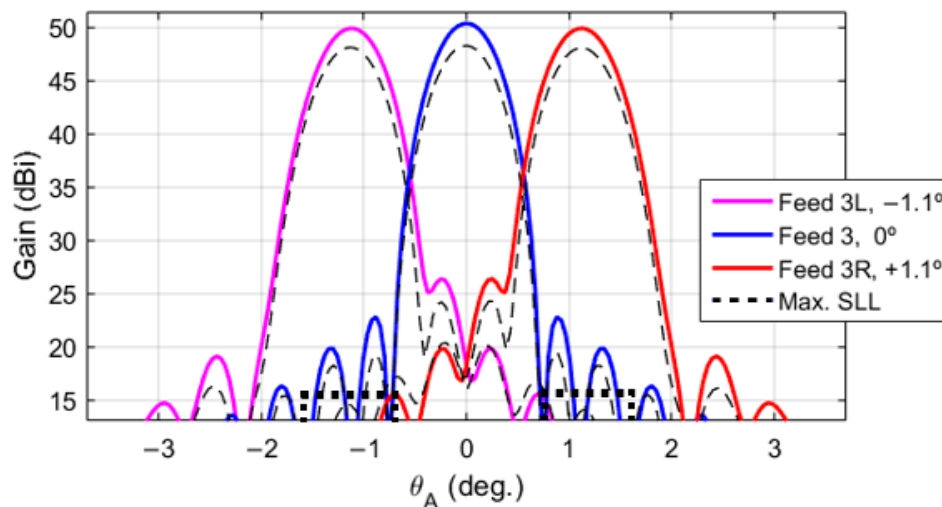


**Figure 7.** Simulated radiation patterns at 20 GHz in the azimuth plane of the beams generated by the bifocal DRAA (solid colored lines) and the beams produced by the equivalent monofocal DRAA (dashed lines), showing the maximum side-lobe levels (SLL, in black dotted lines) that produce the interference among beams with equal polarization.

The amplitude distributions of the incident field on the main-RA produced by the feeds  $F_1$ ,  $F_3$  and  $F_5$  (the two foci of the bifocal antenna and the central feed) are shown in Figure 8. Note that the elliptical illuminations obtained on the main-RA are a consequence of applying the bifocal technique for a high degree of beam spacing reduction in the  $xz$ -plane, which spreads the illumination along the vertical axis of the main-RA, while the illumination along its horizontal axis is determined by the monofocal design (adjusted for a 1.8-m width of the main-RA). The elliptical shape of the main-RA allows obtaining a proper illumination and ensures an acceptable spillover.

The designed bifocal DRAA has been used to produce multiple spots considering the cluster of horns shown in Figure 9a. This cluster includes the five initial feeds, from  $F_1$  to  $F_5$ , and ten additional feeds placed adjacent to the previous ones. The pattern contours of 40 dBi and 47.5 dBi (which is around  $-3$  dB below the maximum gain) for the beams generated by bifocal DRAA at 20 GHz are shown in Figure 9b. The bifocal antenna is able to produce adjacent beams with  $0.56^\circ$  separation in planes " $v = \text{constant}$ ". Due to the use of an elliptical main RA, the antenna generates elliptical spots with a different beamwidth in each of the principal planes (e.g., the beamwidth at 46 dBi gain level for the central beam is  $0.39^\circ \times 0.67^\circ$ ). The interleaved beams required for providing the complete multi-spot coverage will be generated in the orthogonal polarization.

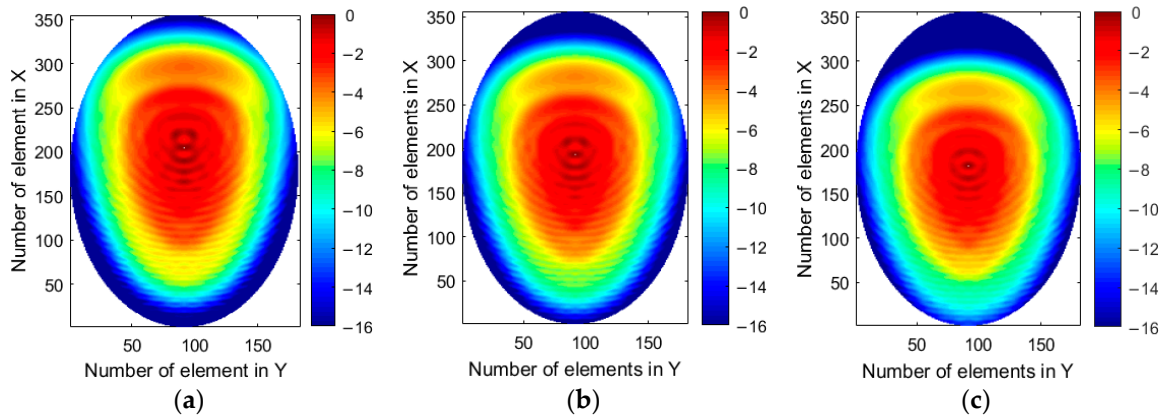


**Figure 8.** Amplitude (in dB) of the incident field on the main RA when the antenna is illuminated from: (a)  $F_1$ , (b)  $F_3$  and (c)  $F_5$ .

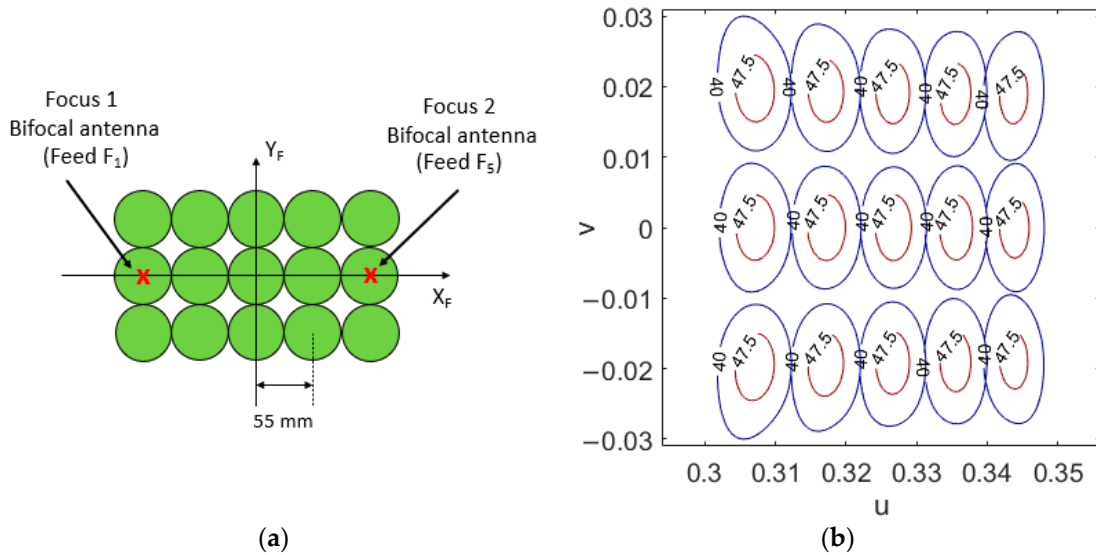


**Figure 9.** (a) Cluster of horns used to illuminate the antenna, including the location of the foci, (b) pattern contours of 40 dBi and 47.5 dBi for the beams produced by the bifocal DRAA at 20 GHz.

#### 4. Design for Dual Polarization

The designed bifocal antenna will be illuminated by a cluster of dual-polarized horns. Each horn will generate two adjacent beams in orthogonal polarization in a plane forming around  $60^\circ$  with respect to the plane “ $v = 0$ ”, in order to produce a complete cellular coverage. The discrimination of the orthogonal polarizations will be performed on the main RA, using reflectarray cells that enable independent phase control in each polarization. Two different phase distributions will be implemented on the main RA (one for each polarization), while the sub-RA will present the same phase distribution for both polarizations (the one shown in Figure 5a).

The phases required on the main RA for the orthogonal polarization can be obtained by adding a progressive phase term to the bifocal phases in Figure 5b. The phase increment at each reflectarray cell can be computed starting from the following expression, which provides the phase distribution of the reflected field on the main RA surface to generate a collimated beam in the direction  $(\theta_b, \varphi_b)$ :

$$\Phi(x_i, y_i) = -k_0 \sin \theta_b (x_i \cos \varphi_b + y_i \sin \varphi_b), \tag{3}$$

where  $x_i$  and  $y_i$  are the coordinates of the  $i$ -element with respect to the main-RA center, and  $k_0$  is the propagation constant in a vacuum. Equation (1) can be adapted to work with the  $(u_b, v_b)$  coordinates associated to the direction of maximum radiation:

$$\Phi(x_i, y_i) = -k_0(x_i \cdot u_b + y_i \cdot v_b). \quad (4)$$

Then, the difference in the required phase shift between two beams whose maximums are located at coordinates  $(u_{b1}, v_{b1})$  and  $(u_{b2}, v_{b2})$  will be:

$$\Delta\Phi(x_i, y_i) = -k_0[x_i \cdot (u_{b2} - u_{b1}) + y_i \cdot (v_{b2} - v_{b1})]. \quad (5)$$

The increment of phase that must be added to the bifocal phases on the main RA to generate the adjacent beams in the orthogonal polarization has been computed cell by cell, using Equation (5) and considering the  $(u, v)$  coordinates associated to the maximums of the beams produced by the central feed. According to Figure 9b, the maximum of the central beam is located at  $(u_{b1} = 0.326, v_{b1} = 0)$ , so the position of the adjacent beam in the orthogonal polarization must be  $(u_{b2} = 0.332, v_{b2} = 0.01)$  in order to produce a triangular spot lattice. The resulting progressive phase distribution to be added to the bifocal phases for the original polarization is depicted in Figure 10a. The pattern contours of 40 dBi and 47.5 dBi for the beams generated at 20 GHz by the bifocal DRAA in the two polarizations are presented in Figure 10b, where illumination from the same cluster of horns (now operating in dual polarization) shown in Figure 9a is considered.

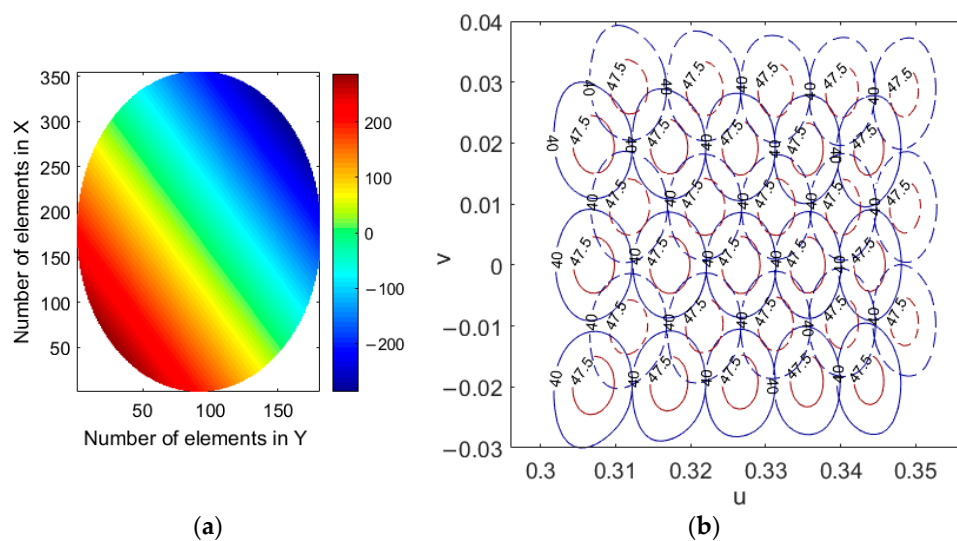


**Figure 10.** Design for dual polarization: (a) phase increment (in degrees) required with respect to the initial polarization and (b) pattern contours of 40 dBi and 47.5 dBi for the beams produced at 20 GHz by the bifocal DRAA, using solid lines for polarization 1 and dashed lines for polarization 2.

The proposed design method is valid for operation in dual linear polarization (LP) or dual circular polarization (CP). In the first case, the reflectarray cells on both the sub-RA and the main RA can be composed of orthogonally-arranged sets of three parallel dipoles, as those shown in Figure 11a. This reflectarray cell allows introducing a different phase shift in each LP (with the incident electric field oriented in the direction of the dipoles) by properly adjusting the lengths of the corresponding group of dipoles. The dipoles are printed on a Di clad 880B dielectric substrate that is backed by a metallic ground plane. The thickness of the substrate is 1.524 mm, the permittivity is  $\epsilon_r = 2.3$  and the loss tangent is  $\tan\delta = 0.001$ . The cell dimensions have been set to  $P_X = P_Y = 7.5$  mm ( $\lambda/2$  at 20 GHz) in order to avoid grating lobes. The width of the dipoles is 0.5 mm, and the separation between the centers of adjacent parallel dipoles is 1 mm.

The surface reflection at the reflectarray cell has been modeled using a matrix formulation that relates the Cartesian components of the incident and reflected tangential electric field. The reflectarray cell is characterized by the reflection matrix ( $R$ ), formed by the co-polar and cross-polar reflection coefficients associated to both polarizations:

$$\begin{pmatrix} E_X^{ref} \\ E_Y^{ref} \end{pmatrix} = \begin{pmatrix} R_{XX} & R_{XY} \\ R_{YX} & R_{YY} \end{pmatrix} \begin{pmatrix} E_X^{inc} \\ E_Y^{inc} \end{pmatrix} \quad (6)$$

where the co-polar reflection coefficients for the X and Y polarizations are represented by  $R_{XX}$  and  $R_{YY}$ , respectively, and the cross-polar coefficients are  $R_{XY}$  and  $R_{YX}$ , respectively. The values of the co- and cross-polar coefficients have been obtained by means of an in-house electromagnetic code that applies the Method of Moments in the spectral domain (SD-MoM). The SD-MoM analysis code assumes that the reflectarray cell is placed in a periodic environment (which is a common approach for the analysis and design of reflectarray antennas [14–20]) and takes into account the real incidence angles on the cell. More details about the in-house SD-MoM code and its validation can be found in [28].

The dual-polarization capability of the reflectarray cell can be explained as follows. The lengths of the dipoles oriented in the direction of the  $x$ -axis will control the phase shift introduced in X-polarization (the phase of the  $R_{XX}$  coefficient), while the lengths of the dipoles oriented in the direction of the  $y$ -axis will adjust the phase shift introduced in Y-polarization (the phase of  $R_{YY}$ ). The lengths of the  $x$ -oriented and  $y$ -oriented dipoles will be separately adjusted to provide the required phase shift in each LP, considering that the lengths of the lateral dipoles are scaled by a factor of 0.78 with respect to the lengths of the central dipoles ( $l_{A1} = 0.78l_{A2}$  and  $l_{B1} = 0.78l_{B2}$ ). The use of orthogonal sets of dipoles results in a very low coupling between the X and Y polarizations [28]. The independent phase control in each polarization provided by the reflectarray cell allows the proposed antenna to generate two independent beams in orthogonal polarization with the same feed.

For a correct design of the reflectarray antenna, a common requirement is that the phase of the co-polar reflection coefficients ( $R_{XX}$  and  $R_{YY}$ ) must present a smooth variation in a range of at least  $360^\circ$ , in order to be able to implement the phase distributions shown in Figure 5. The phase of the  $R_{XX}$  and  $R_{YY}$  coefficients and the amplitude of the cross-polar coefficients ( $R_{XY}$  and  $R_{YX}$ ) at 20 GHz under oblique incidence  $\theta_i = 30^\circ$ ,  $\varphi_i = 30^\circ$  (which are about the maximum incidence angles in the main RA) have been depicted in Figure 11b vs. the length of the central dipole in each polarization (note that the lengths of the lateral dipoles are also varied, according to the relation  $l_{A1/B1} = 0.78l_{A2/B2}$ ). As can be seen, the reflectarray cell provides a satisfactory performance, with around  $400^\circ$  phase range in both polarizations and cross-polar amplitudes below  $-23$  dB for most of the dipole lengths (with a maximum of  $-18$  dB). These results are even better for smaller incidence angles, which will allow obtaining low levels of cross-polar radiation, as can be checked in other reflectarray antennas designed with similar cells based on orthogonal dipoles [20,28]. To achieve simultaneous operation at Tx and Rx frequencies (20/30 GHz), a more complex version of the cell with two layers of stacked dipoles can be used [29]. In that case, the upper dipoles will control the phase response at the higher frequencies, while the lower dipoles will perform the same task at the lower frequencies.

The design of the DRAA to produce the beams in dual-CP presents higher complexity than in the dual-LP case. A possible solution would be to place a linear-to-circular transmission polarizer in front of the main-RA (designed with the previous dual-LP cells based on orthogonal dipoles), as proposed in [30]. In this configuration, the incident field in dual-CP will be converted into dual-LP, and then each LP will be reflected by the main-RA with a different phase shift and converted again into CP. Another alternative would be to use dual-CP feeds and apply the variable rotation technique (VRT) to the reflectarray elements for generating adjacent beams in dual-CP [18] together with variable-size dipoles to provide the required phase-shift, as demonstrated in [31].

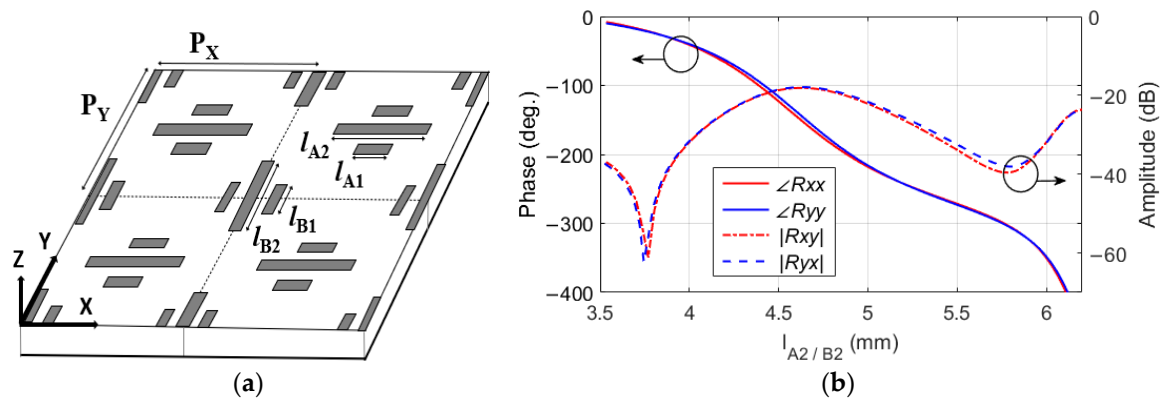


**Figure 11.** (a) Reflectarray cells formed by orthogonal sets of dipoles for controlling each linear polarization (LP):  $2 \times 2$  periodic cells, (b) co-polar reflection phases and cross-polar reflection amplitudes at 20 GHz and under  $\theta_i = 30^\circ$ ,  $\varphi_i = 30^\circ$  oblique incidence.

## 5. Generation of a Complete Multiple Beam Coverage in Ka-Band

The designed bifocal DRAA operating in dual polarization is able to generate a complete multibeam coverage with a single main aperture for transmission in the Ka-band from a GEO satellite. Figure 12 shows the contour patterns and gain levels at 20 GHz associated to the multibeam coverage. These patterns have been obtained using the commercial software SATSOFT [32], developed by TICRA. The input parameters of the software have been configured so that the designed multibeam antenna is placed on board of a GEO satellite (at a distance of 36,000 km from the Earth's surface) and it is properly pointed to illuminate part of the European and North African regions. Then, the radiation patterns of the beams generated by the proposed antenna have been projected over the Earth's surface using the advanced functionalities of SATSOFT. As can be seen in Figure 12, the resulting multibeam coverage is formed by slightly-overlapping elliptical spots arranged in a triangular lattice. The separation between the maximums of adjacent spots is around  $0.56^\circ$ , which is a typical value in current multi-spot applications in Ka-band [3]. The generation of closely-spaced beams is achieved through the application of the bifocal technique to reduce the beam deviation factor in the  $xz$ -plane by 50%, and the discrimination of the orthogonal polarizations at the reflectarray element level.

The proposed bifocal DRAA presents several advantages with respect to the oversized SFPB reflector designed for the same application [5]. The bifocal antenna requires a significantly smaller main aperture (an elliptical reflectarray of  $3.5 \text{ m} \times 1.8 \text{ m}$  instead of a circular reflector with 4 m diameter) and a lower number of feed-horns (reduced by 50% with respect to conventional SFPB reflector systems [3,5], thanks to the dual-polarization capability of reflectarrays). Moreover, the use of flat reflectarray panels, which can be fabricated by conventional photo-etching and processes used in multi-layer printed circuits, allows for more efficient packaging and deployment mechanisms on the satellite. Note that the largest dimension of the main RA matches the maximum aperture size that fits on the spacecraft launcher, which is around 3.5 m [33]. Beyond that size, either mesh unfurlable reflectors or deployable panel reflectors must be employed [33,34].

The aperture efficiency of the proposed multibeam antenna is around 40%, estimated as the ratio between the simulated gain and the maximum directivity associated to the size of the elliptical aperture ( $3.55 \text{ m} \times 1.81 \text{ m}$ ). Note that the generation of a complete multiple spot coverage with a single main aperture prevents the antenna from reaching a high radiation efficiency, because of the use of an oversized aperture. The proposed antenna presents larger aperture efficiency than the oversized SFPB reflector in [5], which shows less than 20% efficiency for a 4-m diameter aperture. Moreover, the efficiency of the proposed DRAA is similar to that of other DRAAs reported in the literature [20,27,35]. Note that the use of the elliptical main RA allows significant reduction of the spillover, which increases the radiation efficiency of the proposed antenna. In the case of using a circular main RA of 1.8 m diameter (instead of the elliptical one), it has been checked that the maximum gain of the beams would

be around 44 dBi, which corresponds to an aperture efficiency below 20%. The antenna would still provide the same beam spacing, because of the bifocal design process, but the large spillover in the main RA would result in low radiation efficiency. On the other hand, the elliptical shape of the main RA matches quite well with the illuminations that are obtained from the feeds, as was shown in Figure 8.

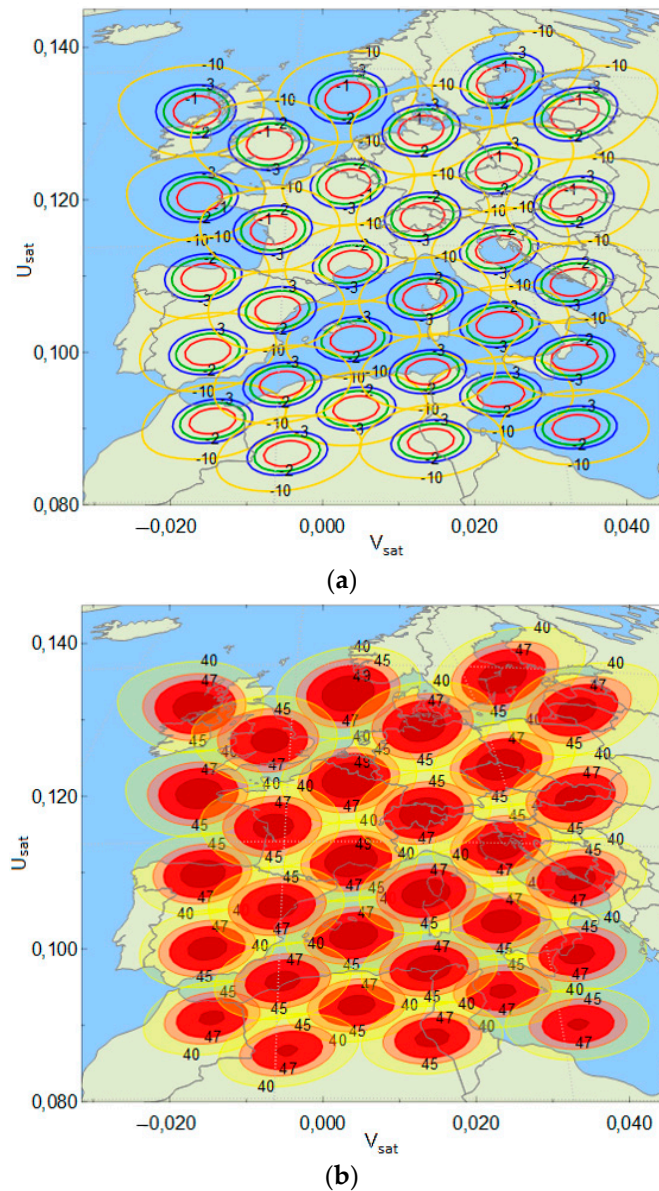


**Figure 12.** Multi-spot coverage produced by the designed DRAA after the projection over the Earth's surface: (a) relative contour patterns and (b) absolute gain levels (in dBi) at 20 GHz.

It is important to note that typical spot beams adopted in a multibeam coverage are circular. However, elliptical spot beams can be considered as well if there is a significant advantage. In the solution proposed in this paper, the advantage is related to the possibility to oversize only one linear dimension of the reflector (instead of oversizing both dimensions, as in [5]), which reduces the overall aperture of the antenna with improvements in terms of accommodation. Due to the elliptical shape of the beams, the adjacent beam overlap in planes " $v = \text{constant}$ " occurs for a gain level around 40.2 dBi, while it is around 45 dBi in the diagonal planes forming  $60^\circ$  with the plane " $v = 0$ " (note that the maximum gain of the spots varies between 49.2 dBi and 50.5 dBi). A similar multi-spot coverage based on elliptical spots arranged in a rectangular lattice has been proposed in [7] for a MFPB reflector

system, but the antenna has the drawback of its greater hardware complexity, due to the use of a MFPB architecture. The performance of the proposed multibeam DRAA could be improved by means of phase optimization techniques, in order to broaden the beams only in one plane, so that the adjacent beam overlap would occur at a higher gain level. For example, phase-only synthesis based on the intersection approach technique [36,37] could be applied to broaden the beams in the elevation plane, without disturbing the bifocal phases that provide the required beam spacing reduction.

The co-polar isolation for the resultant multi-spot coverage has been estimated as the minimum C/I ratio within a 40 dBi gain beamwidth, where the interference is produced by the radiation of the neighbor beams produced in the same combination of frequency and polarization. Some examples of the interference produced among reuse beams are included in Figures 6 and 7. Note that the adjacent feed-horns will alternate in frequency, so the adjacent beams in the same plane “ $v = \text{constant}$ ” (generated in the same polarization by different horns) will alternate in frequency. According to the previous C/I criterion, it has been checked that the co-polar isolation for the multi-spot coverage varies between 17.6 dB and 21.2 dB, which are typical values for practical HTS systems in Ka-band [5]. The design of the bifocal DRAA has been performed at the central frequency of 20 GHz, and it covers the complete frequency range for Tx (19.5–20.5 GHz, a 5% relative bandwidth). Similar and even larger values of bandwidth have been reported in previous works that use reflectarray cells based on orthogonal dipoles [20,28].

## 6. Conclusions

A novel multibeam antenna concept based on a bifocal dual-reflectarray configuration with an elliptical main reflectarray (3.55 m × 1.81 m) has been proposed to generate complete multibeam coverage for transmission from a GEO satellite operating in the Ka-band. The bifocal technique has been applied for the first time to achieve a 50% reduction of the beam deviation factor with respect to the equivalent monofocal antenna. The proposed multibeam antenna requires a smaller main aperture (about half of the area) and shows larger radiation efficiency than other oversized antennas that have been proposed for the same application. An analogous design process can be performed to produce the beams at Rx, if appropriate reflectarray cells that will enable independent phasing at Tx and Rx frequencies are used. The proposed multibeam antenna will allow an important reduction in the volume and weight of the antenna system on board the satellite.

**Author Contributions:** Conceptualization, E.M.-d.-R., J.A.E. and G.T.; methodology, E.M.-d.-R. and J.A.E.; software, E.M.-d.-R.; validation, E.M.-d.-R. and J.A.E.; investigation, E.M.-d.-R. and J.A.E.; writing—original draft preparation, E.M.-d.-R.; writing—review and editing, J.A.E. and G.T.; visualization, E.M.-d.-R. and J.A.E.; supervision, J.A.E. and G.T.; project administration, J.A.E. and G.T.; funding acquisition, J.A.E. and G.T. All authors have read and agreed to the published version of the manuscript.

**Funding:** This research was funded by the European Regional Development Fund and the Spanish Ministry of Economy and Competitiveness, under Project TEC2016-75103-C2-1-R, and by the European Space Agency ESTEC, under Contract 4000117113/16/NL/AF.

**Conflicts of Interest:** The authors declare no conflict of interest.

## References

1. Fenech, H.; Amos, S.; Tomatis, A.; Soumpholphakdy, V. High throughput satellite systems: An analytical approach. *IEEE Trans. Aerosp. Electron. Syst.* **2015**, *51*, 192–202. [[CrossRef](#)]
2. Rao, S.K. Advanced antenna technologies for satellite communications payloads. *IEEE Trans. Antennas Propag.* **2015**, *63*, 1205–1217. [[CrossRef](#)]
3. Schneider, M.; Hartwanger, C.; Wolf, H. Antennas for multiple spot beams satellites. *CEAS Space J.* **2011**, *2*, 59–66. [[CrossRef](#)]
4. Toso, G.; Mangenot, C. Angeletti, Recent advances on space multibeam antennas based on a single aperture. In Proceedings of the 2013 7th European Conference on Antennas and Propagation (EuCAP), Gothenburg, Sweden, 8–12 April 2013.

5. Balling, P.; Mangenot, C.; Roederer, A.G. Shaped single-feed-per-beam multibeam reflector antenna. In Proceedings of the 2006 First European Conference on Antennas and Propagation, Nice, France, 6–10 November 2006.
6. Schneider, M.; Hartwanger, C.; Sommer, E.; Wolf, H. Test results for the multiple spot beam antenna project Medusa. In Proceedings of the 4th Eur. Conf. Antennas and Propag. (EuCAP), Barcelona, Spain, 6–10 November 2006.
7. Bosshard, P. Thales Alenia Space HTS/V-HTS multiple beam antennas sub-systems on the right track. In Proceedings of the 2016 10th European Conference on Antennas and Propagation (EuCAP), Davos, Switzerland, 10–15 April 2016.
8. Bucci, O.M.; Isernia, T.; Perna, S.; Pinchera, D. Isophoric sparse arrays ensuring global coverage in satellite communications. *IEEE Trans. Antennas Propag.* **2014**, *62*, 1607–1618. [[CrossRef](#)]
9. Cailloce, Y.; Caille, G.; Albert, I.; Lopez, J.M. A Ka-band direct radiating array providing multiple beams for a satellite multimedia mission. In Proceedings of the 2000 IEEE International Conference on Phased Array Systems and Technology (Cat. No.00TH8510), Dana Point, CA, USA, 21–25 May 2000.
10. Ruggerini, G.; Nicolaci, G.; Toso, G.; Angeletti, P. A Ka-band active aperiodic constrained lens antenna for multibeam applications: Active discrete lens antennas are promising alternative solutions for multibeam coverage using a single aperture. *IEEE Antennas Propag. Mag.* **2019**, *61*, 60–68. [[CrossRef](#)]
11. Lian, J.-W.; Ban, Y.-L.; Zhu, H.; Guo, Y.J. Reduced-sidelobe multibeam array antenna based on SIW Rotman lens. *IEEE Antennas Wireless Propag. Lett.* **2020**, *19*, 188–192. [[CrossRef](#)]
12. Doucet, F. Shaped continuous parallel plate delay lens with enhanced scanning performance. *IEEE Trans. Antennas Propag.* **2019**, *67*, 6695–6704. [[CrossRef](#)]
13. Chou, H.-T.; Yan, Z.-D. Parallel-plate Luneburg lens antenna for broadband multibeam radiation at millimeter-wave frequencies with design optimization. *IEEE Trans. Antennas Propag.* **2018**, *66*, 5794–5804. [[CrossRef](#)]
14. Rengarajan, S.R. Reflectarrays of rectangular microstrip patches for dual-polarization dual-beam radar interferometers. *Prog. Electromagn. Res.* **2013**, *133*, 1–15. [[CrossRef](#)]
15. Mener, S.; Gillard, R.; Sauleau, R.; Bellion, A.; Potier, P. Dual circularly polarized reflectarray with independent control of polarizations. *IEEE Trans. Antennas Propag.* **2015**, *63*, 1877–1881. [[CrossRef](#)]
16. Smith, T.; Gothelf, U.; Kim, O.S.; Breinbjerg, O. An FSS-backed 20/30 GHz circularly polarized reflectarray for a shared aperture L- and Ka-band satellite communication antenna. *IEEE Trans. Antennas Propag.* **2014**, *62*, 661–668. [[CrossRef](#)]
17. Chaharmir, M.R.; Shaker, J. Design of a multilayer X/Ka-band frequency-selective surface-backed reflectarray for satellite applications. *IEEE Trans. Antennas Propag.* **2015**, *63*, 1255–1264. [[CrossRef](#)]
18. Zhou, M.; Sørensen, S.B. Multi-spot beam reflectarrays for satellite telecommunication applications in Ka-band. In Proceedings of the 2016 10th European Conference on Antennas and Propagation (EuCAP), Davos, Switzerland, 10–15 April 2016.
19. Naseri, P.; Hum, S.V. A dual-band dual-circularly polarized reflectarray for K/Ka-band space applications. In Proceedings of the 2019 13th European Conference on Antennas and Propagation (EuCAP), Krakow, Poland, 31 March–5 April 2019.
20. Martinez-de-Rioja, E.; Encinar, J.A.; Florencio, R.; Tienda, C. 3-D bifocal design method for dual-reflectarray configurations with application to multi-beam satellite antennas in Ka-band. *IEEE Trans. Antennas Propag.* **2019**, *67*, 450–460. [[CrossRef](#)]
21. Rao, B.L. Bifocal dual reflector antenna. *IEEE Trans. Antennas Propag.* **1974**, *22*, 711–714. [[CrossRef](#)]
22. Rappaport, M. An offset bifocal reflector antenna design for wide-angle beam scanning. *IEEE Trans. Antennas Propag.* **1984**, *32*, 1196–1204. [[CrossRef](#)]
23. Garcia-Pino, A. Bifocal reflector antenna for a standoff radar imaging system with enhanced field of view. *IEEE Trans. Antennas Propag.* **2014**, *62*, 4997–5006. [[CrossRef](#)]
24. Plastikov, A.N. A high-gain multibeam bifocal reflector antenna with 40° field of view for satellite ground station applications. *IEEE Trans. Antennas Propag.* **2016**, *64*, 3251–3254. [[CrossRef](#)]
25. La, T.V.; Nguyen, N.T.; Casaletti, M.; Sauleau, R. Design of medium-size dielectric bifocal lenses for wide-angle beam scanning antennas. In Proceedings of the 2012 6th European Conference on Antennas and Propagation (EuCAP), Prague, Czech Republic, 26–30 March 2012.

26. Menzel, W.; Al-Tikriti, M.; Leberer, R. A 76-GHz multiple-beam planar reflector antenna. In Proceedings of the 2002 32nd European Microwave Conference, Milan, Italy, 23–26 September 2002.
27. Tienda, C.; Encinar, J.A.; Arrebola, M.; Barba, M.; Carrasco, E. Design manufacturing and test of a dual-reflectarray antenna with improved bandwidth and reduced cross-polarization. *IEEE Trans. Antennas Propag.* **2013**, *61*, 1180–1190. [[CrossRef](#)]
28. Florencio, R.; Encinar, J.A.; Boix, R.R.; Losada, V.; Toso, G. Reflectarray antennas for dual polarization and broadband Telecom satellite applications. *IEEE Trans. Antennas Propag.* **2015**, *63*, 1234–1246. [[CrossRef](#)]
29. Martinez-de-Rioja, E.; Encinar, J.A.; Florencio, R.; Boix, R.R. Reflectarray in K and Ka bands with independent beams in each polarization. In Proceedings of the 2016 IEEE International Symposium on Antennas and Propagation (APSURSI), Fajardo, PR, USA, 26 June–1 July 2016.
30. Hosseini, M.; Hum, S.V. A dual-CP reflectarray unit cell for realizing independently controlled beams for space applications. In Proceedings of the 2017 11th European Conference on Antennas and Propagation (EUCAP), Paris, France, 19–24 March 2017.
31. Florencio, R.; Encinar, J.A.; Boix, R.R.; Barba, M.; Toso, G. Flat reflectarray that generates adjacent beams by discriminating in dual circular polarization. *IEEE Trans. Antennas Propag.* **2019**, *67*, 3733–3742. [[CrossRef](#)]
32. SATSOFT-TICRA: Coverage Planning Software. Available online: <https://www.ticra.com/software/satsoft> (accessed on 30 May 2020).
33. Palacin, B. Multibeam antennas for very high throughput satellites in Europe: Technologies and trends. In Proceedings of the 2017 11th European Conference on Antennas and Propagation (EUCAP), Paris, France, 19–24 March 2017.
34. Di Bari, R.; Albert, B.; Abunjaileh, A. Ka-band multibeam antenna development for VHTS. In Proceedings of the 12th European Conference on Antennas and Propagation (EuCAP 2018), London, UK, 9–13 April 2018.
35. Zhao, J. A low-mutual coupling dual-band dual-reflectarray antenna with the potentiality of arbitrary polarizations. *IEEE Antennas Wireless Propag. Lett.* **2017**, *16*, 3224–3227. [[CrossRef](#)]
36. Bucci, O.; Franceschetti, G.; Mazzarella, G.; Panariello, G. Intersection approach to array pattern synthesis. *Proc. Inst. Elect. Eng.* **1990**, *137*, 349–357. [[CrossRef](#)]
37. Zornoza, A.; Encinar, J.A. Efficient phase-only synthesis of contoured beam patterns for very large reflectarrays. *Int. J. RF Microw. Comput. Aided Eng.* **2004**, *14*, 415–423. [[CrossRef](#)]



© 2020 by the authors. Licensee MDPI, Basel, Switzerland. This article is an open access article distributed under the terms and conditions of the Creative Commons Attribution (CC BY) license (<http://creativecommons.org/licenses/by/4.0/>).